RSC Advances

RSC Publishing

PAPER

View Article Online
View Journal | View Issue

Cite this: *RSC Adv.*, 2013, **3**, 22597

Microwave-assisted synthesis of nitrogen and boron co-doped graphene and its application for enhanced electrochemical detection of hydrogen peroxide†

Guo-Hai Yang, Yu-Hui Zhou, Jia-Jun Wu, Jun-Tao Cao, Ling-Ling Li, Hong-Ying Liu and Jun-Jie Zhu*

Received 9th August 2013
Accepted 25th September 2013

DOI: 10.1039/c3ra44284e

www.rsc.org/advances

A microwave-assisted strategy was developed for the synthesis of nitrogen and boron co-doped graphene (NB-G) with a hierarchical framework, and the NB-G was characterized by transmission electron microscopy, scanning electron microscopy, X-ray photoelectron spectroscopy and Raman spectroscopy. The resultant NB-G network provided multidimensional electron transport pathways, and was used in the electrocatalytic reduction for hydrogen peroxide (H_2O_2) sensing, exhibiting an excellent response and stability. The NB-G modified electrochemical sensor showed a linear range from 0.5 μM to 5 mM with a detection limit of 0.05 μM at a signal-to-noise ratio of 3. This high performance was attributed to both the beneficial structure of NB-G and synergetic effects arising from the co-doping of N and B in graphene. The proposed biosensor was also used to achieve real-time quantitative detection of H_2O_2 from living cells at the nanomolar level, which exhibited excellent electrochemical activity.

1. Introduction

Hydrogen peroxide (H_2O_2), is known as a by-product of aerobic respiration and a part of the phagocytic respiratory burst, and has recently been shown to be a messenger in cellular signal transduction.[1] The emerging concept of H_2O_2 as a redox signal that triggers reversible post translational modification of precise protein targets has generated interests in understanding how cells produce, partition and funnel H_2O_2 into specific signaling pathways.[2,3] As a reactive oxygen species (ROS), H_2O_2 also plays an important role in many oxidative biological reactions as an essential mediator, including those catalyzed by glucose oxidase, cholesterol oxidase and alcohol oxidase, *etc.* Over-production of H_2O_2 can lead to oxidative stress and subsequent functional decline in organ systems, inducing neurodegeneration or cancer.[4,5] Thus, the precise and rapid detection of H_2O_2 is of significant importance. To better understand the biological effects of H_2O_2, it is critically important to monitor H_2O_2 levels in biological environments, especially in the cellular environment, and new diagnostic methods are needed to detect and quantify endogenous H_2O_2 production. H_2O_2 has been detected by various methods,[6–9] among which electrochemical method has become increasingly attractive in biological applications because it possesses better temporal resolution for measurements, offering great potential to image the dynamic release process of H_2O_2.[10] However, most amperometric techniques rely on enzyme-based biosensors which have intrinsic problems such as poor enzyme stability and interference from electroactive species. Therefore, it is important to fabricate a novel low cost electrode material for the oxidation of H_2O_2 and develop a highly selective and sensitive H_2O_2 sensor to track the role of H_2O_2 in physiological and pathological processes.

Nanomaterials have attracted significant attention due to their outstanding properties. Previous reports have shown that carbon-based nanocomposites possess good sensing ability for H_2O_2 and can efficiently improve electron transfer between the analyte and electrode.[11,12] Since first discovered by Novoselov *et al.*,[13] graphene, which has a unique structure of two-dimensional sheets composed of sp^2-bonded carbon atoms, has fascinated many researchers in numerous fields because of its extraordinary physical and chemical properties, such as high carrier mobility, excellent thermal conductivity and specific surface area.[14–17] Both theoretical and experimental studies[18–23] revealed that chemical doping with heteroatoms, such as nitrogen (N), boron (B) or sulfur atoms, was an effective method for tailoring the electrical properties of graphene for more widespread applications. Doped graphene has been intensively investigated as an electrode material for supercapacitors, lithium-ion batteries and oxygen reduction reactions.[24–29] Recently, graphene co-doped with two elements has also shown much better performance than single doped graphene for fuel cells and energy storage, and this has become one of the main trends in the tailoring of its chemical and physical properties

State Key Laboratory of Analytical Chemistry for Life Science, School of Chemistry and Chemical Engineering, Nanjing University, Nanjing, 210093, P. R. China. E-mail: jjzhu@nju.edu.cn; Fax: +86-25-8359-7204; Tel: +86-25-8359-7204

† Electronic supplementary information (ESI) available: Fig. S1–S4. See DOI: 10.1039/c3ra44284e

for desired purposes.[30–33] Moreover, achieving positive architectures of graphene-based materials is vital for macroscopic applications.[34] Consequently, the identification of a simple and effective strategy to synthesize co-doped graphene with a beneficial structure is highly desirable. On the other hand, little attention has been paid to enhancing the performance of co-doped graphene in electrochemical sensing, and it has been demonstrated that N or B doping could enhance the biocompatibility and sensitivity of carbon nanotubes in biosensing applications.[35,36] Therefore, a study on the synthesis of N and B co-doped graphene (NB-G) and exploring its potential in biological fields is a valuable and crucial topic.

Herein, we developed a novel microwave-assisted strategy for the synthesis of NB-G with a hierarchical framework. The as-prepared NB-G offered a large active surface area, high conductivity and unhindered substance diffusion, and was investigated as an excellent material for enzyme-free biosensors. H_2O_2 showed a better electrochemical response at the NB-G modified glassy carbon electrode (GCE), much higher than that of graphene solely doped with N atoms (N-G) or with B atoms (B-G) due to a synergistic effect between the heteroatoms, and a sensitive H_2O_2 amperometric sensor was fabricated with significantly improved sensitivity, selectivity and stability. Finally, the developed method, with theoretical simplicity, and less technical and instrumental demands, was successfully used in the reliable detection of H_2O_2 released from live cells. This technique was a simple and reliable approach for monitoring ROS in biological systems, which may be related to physiological and pathological events.

2. Experimental section

2.1. Materials and apparatus

Cyanamide, B_2O_3 and H_2O_2 (30%) were purchased from Alfa-Aesar. Graphite powder, *N*-formylmethionyl-leucyl-phenylalanine (fMLP) and catalase were supplied by Sigma-Aldrich. All other chemicals used were of analytical reagent grade. The deionized water was obtained from a Millipore Autopure system and used in all experiments. Phosphate buffer solutions (PBS) of various pH values were prepared by mixing the stock solutions of NaH_2PO_4 and Na_2HPO_4, and then adjusting the pH with NaOH and H_3PO_4.

Transmission electron microscopy (TEM) and high-resolution transmission electron microscopy (HRTEM) were performed on a JEOL 2100 transmission electron microscope using an accelerating voltage of 200 kV. High-angle annular dark-field scanning TEM (HAADF-STEM) images and element analysis mapping were carried out on a JEOL JEM-2100F electron microscope operated at 200 kV. Scanning electron microscopy (SEM) images were obtained with a Hitachi S-4800 scanning electron microscope. Atomic force microscopy (AFM) was carried out using an Agilent 5500 atomic force microscope operated in tapping mode with sample on freshly cleaved mica. The X-ray photoelectron spectroscopy (XPS) measurements were obtained using a commercial XPS system (PHI 5000 Versa Probe) equipped with a hemispherical electron analyser and monochromatic Al Kα X-ray excitation source. The specific surface area of the catalysts was calculated using the Brunauer–Emmett–Teller (BET) equation. The nitrogen adsorption–desorption data were recorded in liquid nitrogen at a temperature of 77 K using Micromeritics ASAP 2020M apparatus. Before the measurements were performed, the samples were incubated for 10 h at 300 °C. Fourier transform infrared spectroscopy (FT-IR) analyses were carried out by KBr pellet and carried out using a Nicolet 6700 FT-IR spectrometer. Raman spectra were conducted on a Renishaw *via* Raman microscope equipped with a ×50 objective and 514.5 nm diode laser excitation on a 1800-line grating. X-ray powder diffraction (XRD) was performed on a XRD-6000 (Shimadzu) using Cu Kα (0.15406 nm) radiation with the sweeping rate of 5° per minute. Thermogravimetric analysis (TGA) was performed using Pyres 1 apparatus (Perkin Elmer, MA, USA) at a heating rate of 10 °C min^{-1} from room temperature to 1000 °C under a nitrogen atmosphere.

2.2. Synthesis of NB-G

Graphene oxide (GO) was synthesized through the oxidative treatment of purified natural graphite using a previously reported method (see in ESI†).[37] Then 50 mL of GO (1.0 mg mL^{-1}) aqueous dispersion mixed with 5.0 mL of 50% cyanamide solution was first treated with microwave for 1 h, and dried under vacuum at 60 °C for several hours. The powder was then ground with B_2O_3, the sample was placed in a quartz boat and introduced into the middle of a tube furnace, and pyrolysis was performed at 900 °C for 0.5 h in an Ar atmosphere. For comparison, N-G and B-G were prepared using cyanamide as N precursor and B_2O_3 as B precursor, respectively. The pristine graphene (G) was also prepared in the absence of doping precursor.

2.3. Cells and culture

The CCRF-CEM leukemia cell line from Nanjing KeyGen Biotech Co. Ltd. was cultured in RPMI 1640 medium (Gibco, Grand Island, NY) supplemented with 10% fetal calf serum (HyClone Laboratories Inc., Logan, UT), penicillin (100 units mL^{-1}) and treptomycin (100 μg mL^{-1}). The cells were grown in standard 100 × 20 mm^2 Petri dishes (Corning Inc., Corning, NY) at 37 °C in a humidified incubator containing 5% CO_2. At the logarithmic growth phase, the cells were collected and separated from the medium by centrifugation at 1000 rpm for 6 min, washed three times with sterile PBS at pH 7.4, and then resuspended in cold PBS containing 1.0 mM Ca^{2+} and 1.0 mM Mn^{2+}. The cell number was obtained using a Petroff-Hausser cell counter.

2.4. Electrochemical experiments

Electrochemical experiments were performed on an electrochemical analyzer (CHI 660C, CHI Instrument) using a standard three electrode cell. A platinum wire was used as the counter electrode and a saturated calomel electrode (SCE) as the reference electrode. The GCE was successively polished using 1.0 and 0.3 μm alumina powder followed by rinsing thoroughly with deionized water. After successive sonication in 1 : 1 nitric acid, acetone and deionized water, the electrode was rinsed with

deionized water and dried at room temperature. A suspension of the catalyst at a concentration of 1.0 mg mL^{-1} was obtained by ultrasonically dispersing the catalyst into chitosan solution (0.5 wt% with 2% acetic acid). The suspension (10 μL) was then dropped onto the GCE and dried thoroughly in air. Electrochemical reduction of H_2O_2 was monitored under a saturated N_2 condition using 2.5 mM H_2O_2. Amperometric measurements were performed at −0.25 V in the N_2-saturated 0.1 M PBS (pH 7.4) solution.

2.5. Measuring the H_2O_2 released from living CCRF-CEM cells

After growing to 90% confluence, the cells were collected and washed for three times with PBS. The cell number was estimated using a hemocytometer. After centrifugation, a cell-packed pellet was obtained, and 10 mL PBS (pH 7.4) was added for the electrochemical experiments. Prior to the measurements, the buffer was deoxygenated under a nitrogen stream. The potential for modified electrode was controlled at −250 mV (*vs.* Ag/AgCl). After a steady background was obtained, 1.0 μM fMLP was added and the response current was recorded at 37 °C.

3. Results and discussions

3.1. Fabrication and characterization of NB-G

Heteroatom modification is a popular approach to intrinsically modify the properties of host materials. Nitrogen and/or boron doping in carbon networks can effectively tune the electronic properties. In this strategy, a two-step procedure is employed to synthesize NB-G to avoid the BN structure with electrochemical inactivity.[38,39] Cyanamide and B_2O_3 were selected as N and B precursors, respectively to achieve high doping contents in the fabrication of NB-G. Scheme 1 describes the process of NB-G synthesis. Firstly, the GO dispersion was mixed with cyanamide and treated at 160 °C and 180 psi for 1 h under microwave irradiation (200 W) in the cavity of a microwave oven (CEM Discover, USA). The dried mixture was then ground by mortar with B_2O_3, heated to 900 °C at a rate of 10 °C min^{-1} and kept for 0.5 h under an Ar atmosphere in a corundum tube furnace. The resultant powder was finally washed and filtered several times with hot deionized water to remove the residual B_2O_3. N-G, B-G and G were also prepared under similar condition for comparison.

Microwave irradiation is fast and highly efficient for transferring energy into the reaction system, the temperature increases uniformly throughout the reactants,[40] and it has been applied in graphene synthesis for energy storage.[41] Herein, microwave treatment followed by high-temperature annealing in an inert atmosphere prompted the conversion of GO to NB-G, and NB-G spontaneously self-assembled into an ordered structure. The as-prepared NB-G framework was first investigated by TEM and SEM images. Fig. 1A clearly shows that the GO sheets have two-dimensional structures, indicating the exfoliated nanoplatelet texture characteristic of graphene. The NB-G was crumpled with wrinkles and ripples on the surface (Fig. 1B), due to polymerization of the adsorbed cyanamide on doped graphene during the microwave and thermal processes. Cyanamide also acted as a swelling agent to effectively prevent GO from self-stacking during the reaction. Continuous cross-linked networks and abundant hierarchical structures were observed in the SEM image (Fig. 1D). More images are shown in Fig. S1 in the ESI.† However, the hierarchical structure was not observed using the conventional heating method (Fig. S2†). The HRTEM image also revealed the few-layer planar structure (Fig. 1C), which was identified as graphene sheets viewed on the edge. To determine the crystallinity of the NB-G hierarchical structure, the selected-area electron diffraction (SAED) pattern was also examined (inset in Fig. 1C), where one set of well-defined hexagonal diffraction spots was detected, corresponding to the typical hexagonal lattice of carbon within the graphite plane.[42] The result indicated that the as-prepared NB-G had good crystallinity.

To obtain insight into the distribution of C, N and B in the NB-G, STEM was carried out for elemental analysis (Fig. 2a) with

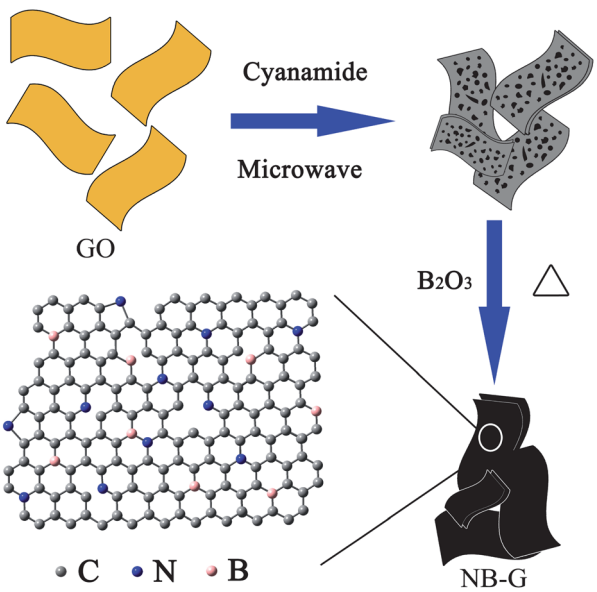

Scheme 1 Fabrication of NB-G framework from GO.

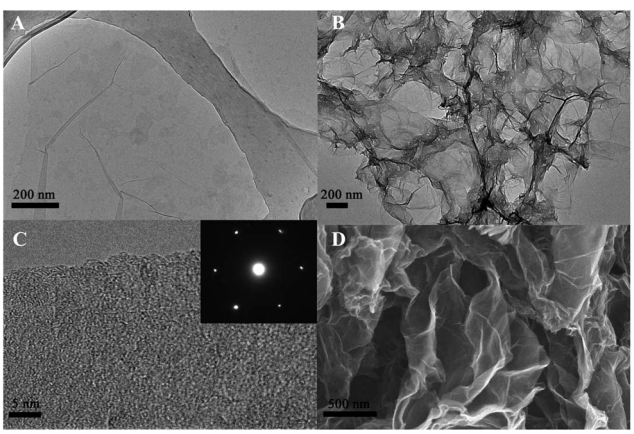

Fig. 1 TEM images of GO (A) and NB-G (B). (C) HRTEM image of NB-G (the inset shows the SAED pattern of the lattice domain). (D) Typical SEM image of NB-G.

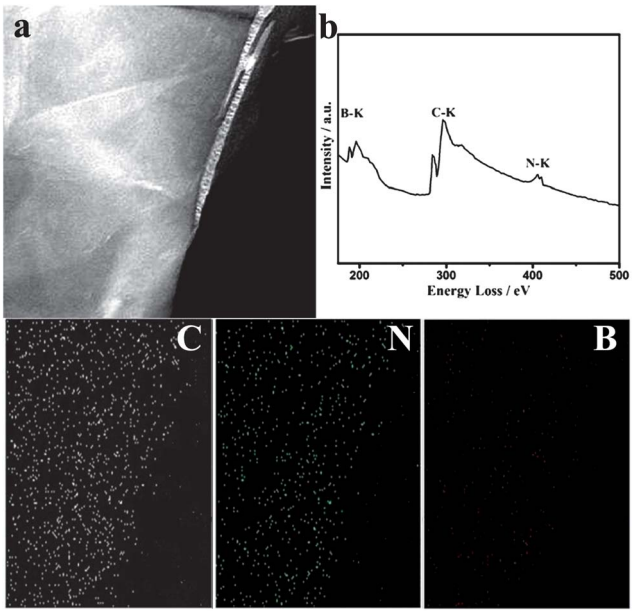

Fig. 2 (a) HAADF STEM image of NB-G, and the corresponding elemental mapping images. (b) The EELS spectrum of NB-G.

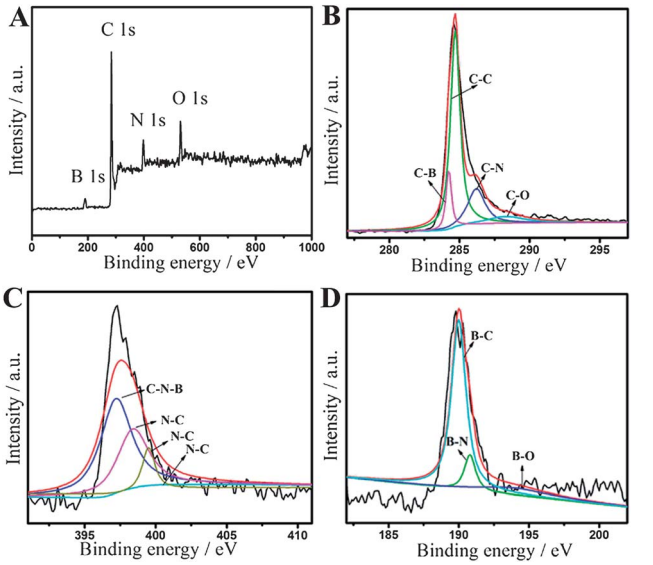

Fig. 3 (A) XPS spectrum of NB-G. The corresponding high-resolution XPS spectra of C_{1s} (B), N_{1s} (C) and B_{1s} (D).

the corresponding elemental mapping images of C, N and B in a selected area of the atomic film, which showed that all three elements were distributed in the imaged area. Electron energy loss spectroscopy (EELS) was used to characterize the K-edge absorption of C, N and B. Fig. 2b shows the typical EELS spectra from an individual NB-G. Three distinct absorption features at 284, 403 and 188 eV corresponded to the expected C, N and B K-edges respectively,[43] indicating the successful incorporation of C, N and B in the NB-G framework.

Strong evidence for the substitutional incorporation of N and B dopants into the graphite lattice of graphene was also provided by XPS. As shown in Fig. 3A, the survey scan spectrum for NB-G exhibited C_{1s} (~284.3 eV), N_{1s} (~400.0 eV), B_{1s} (~190.0 eV) and O_{1s} peaks (~531.0 eV), with significant contents of N (7.1% atomic percent) and B (3.9% atomic percent). Previous studies reported that the introduction of foreign atoms could increase the number of hole-type charge carriers to enhance the conductivity. When the doping amount was increased to some content, heavily co-doped graphene might be a superconductor[44] and could facilitate electrochemical activity. Fig. 3 also shows the corresponding high-resolution XPS results for C, N and B in NB-G. The four deconvoluted peaks in the C_{1s} spectrum at 283.4, 284.7, 286.2 and 288.3 eV could be assigned to C–B, C–C, C–N and C–O bonds, respectively (Fig. 3B).[25] The high-resolution N_{1s} spectrum in Fig. 3C could be deconvoluted into four subpeaks at 398.2, 399.5, 401.1 and 402.6 eV, corresponding to the C–N–B, pyridine N–C, pyrrole N–C and graphitic N–C bonds, respectively.[27] The broad band of B_{1s} could be deconvoluted into two main bands at 189.9 and 191.0 eV (Fig. 3D), which were assigned to the B–C and B–N bonding structures,[45] respectively. It is reasonable to conclude that N and B atoms were introduced into the carbon framework *via* covalent bonds.[46] The decrease in electron density of the substitutional N and B atoms was accompanied by an increase in the electron density on nearby active carbon sites. It is expected that doping plays an important role in regulating the electronic properties and enhancing the electrocatalytic activity of graphene in the electrochemical system.

The structure was also revealed using typical AFM images. Fig. S3† shows that the thickness of the GO nanosheets is approximately 1.0 nm for the presence of covalently bound oxo-groups, indicating the monolayer structure. The NB-G hierarchical framework on the edge still maintained their lateral shape with an average thickness of 0.8 nm (Fig. 4A), confirming the few-layer feature.[29,47]

Nitrogen adsorption–desorption analysis displayed a typical BET surface area of up to 305.0 $m^2 g^{-1}$ for the NB-G hierarchical framework (Fig. 4B), with an average pore size of around 22.4 nm, higher than that of the sample prepared using conventional heating method followed by high-temperature annealing (85.6 $m^2 g^{-1}$). This might be ascribed to the thermally unstable oxygen-containing groups on graphene sheets generated under microwave treatment, which decomposed into CO and/or CO_2 at elevated temperature, and created additional micropores and exerted a driving force for expansion and exfoliation of the aggregated graphene sheets.[41] Thus the NB-G network not only preserved the excellent electrical properties, but also resulted in an high surface area.

Fig. 4C displays the typical FT-IR spectra before and after N and B incorporation. GO exhibited oxygen-containing groups (C=O at 1739 cm^{-1} and C–O at 1230 cm^{-1}),[48] while for NB-G, the obvious decrease in the oxygenated functional groups showed the reduction of GO, and the C=C bands at ~1600 cm^{-1} representing graphitic backbone became more intense for NB-G, suggesting successful reduction and high graphene purity.[48] The appearance of C–N and C–B chemical bonds suggested N and B were successfully coupled with C.

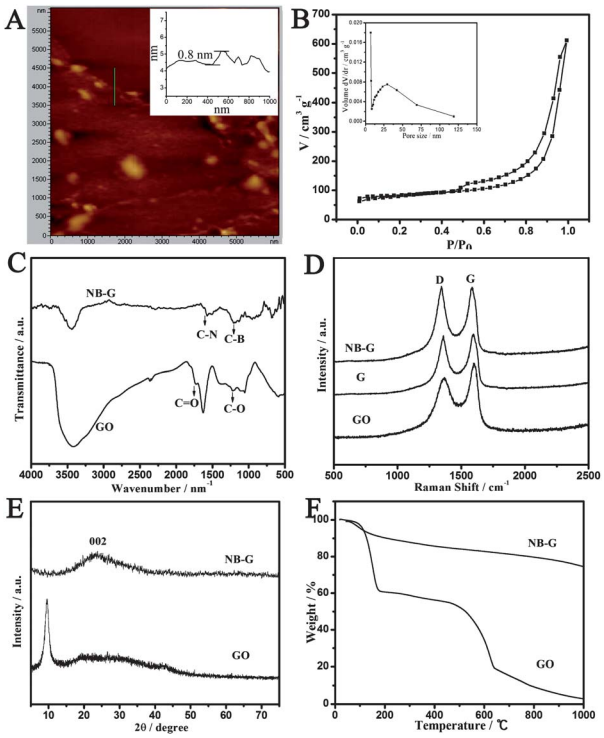

Fig. 4 (A) AFM image of NB-G. (B) Nitrogen adsorption-desorption isotherm of NB-G (The inset shows the pore size distribution). (C) FT-IR spectra of GO and NB-G. (D) Raman spectra of GO, G and NB-G. (E) XRD pattern of GO and NB-G. (F) TGA curves of GO and NB-G.

Raman spectra of the samples were collected on a micro-Raman spectrometer at an excitation wavelength of 514 nm under ambient conditions by dropping the DMF dispersions on mica substrates. Fig. 4D displays the typical Raman spectra for GO, G and the NB-G. The peaks at around 1368 and 1598 cm^{-1} corresponded to the D and G bands, respectively. The G band is attributed to in-plane bond stretching of pairs of sp^2 C atoms and the D mode is associated with defects or lattice distortion.[49] The intensity ratio of D band to G band (I_D/I_G) for G was higher than GO, probably due to the generation of smaller nano-crystalline graphene domains. Following co-doping with N and B, the intensity ratio of I_D/I_G increased further, suggesting increased structural disorder.[30,31]

The crystalline structure of NB-G was further characterized by XRD. In Fig. 4E, the feature diffraction peak of GO at 10.4° (002) was observed with an interlay space (*d*-spacing) of 0.76 nm,[50] suggesting the complete exfoliation of graphite. For NB-G, the peak at 10.4° vanished and a new broad peak at 24.4° appeared with a *d*-spacing of 0.36 nm, which corresponded to the (002) plane of graphene, indicating that the fabrication process could partially restore the graphitic crystal structure due to the reduction effect of high temperature and co-doping,[51] consistent with the HRTEM results.

TGA was also used to examine the thermal stability of the as-prepared NB-G compared to GO (Fig. 4F), recorded in an N_2 atmosphere. GO was thermally unstable and started to lose mass upon heating below 100 °C due to adsorbed water. There were two significant drops in mass around 200 and 500 °C, which were assigned to evolution of the oxygen-containing functional groups and combustion of the carbon skeleton of GO, respectively. In general, NB-G was found to be stable up to 1000 °C, indicating excellent thermal stability. Hence NB-G with versatile properties which was prepared by a convenient, economical and scalable method, and the method may also be a good candidate for numerous applications.

3.2. Electrochemical performance of NB-G modified GCE

Different from the conventional 2D stacked graphene film, NB-G provides a hierarchical framework with maximum access to the doping sites within highly exposed graphene sheets and multidimensional electron transport pathways.[34] To investigate the effect of NB-G on electron transfer kinetics of the redox probe at the electrode, the cyclic voltammograms (CVs) of NB-G modified GCE (NB-G/GCE), together with G/GCE, B-G/GCE and N-G/GCE, in 0.1 M KCl solution containing 2 mM $K_3[Fe(CN)_6]$/$K_4[Fe(CN)_6]$, are shown in Fig. 5. The peak current of NB-G/GCE was higher than that of G/GCE, B-G/GCE and N-G/GCE, and the potential difference of the peak-to-peak at NB-G/GCE was small. These results showed that NB-G effectively accelerated electron transfer between $Fe(CN)_6^{3-/4-}$ and the electrode. With the above advantages, NB-G was selected an candidate to develop as a sensitive platform for biosensing.

Graphene-based composites demonstrate good performance in the detection of some important targets.[52–54] In the present study, to explore the application of NB-G in electrochemical sensing, the CV characteristics of H_2O_2 at the NB-G modified electrode were investigated. Sensitive detection of H_2O_2 is important because it is widely used in many fields such as food, biological and environmental analyses. In our electrochemical experiments, the chemical reaction proceeded as the following equation: $H_2O_2 + 2e^- \rightarrow 2OH^-$. Fig. 6 shows the typical CVs obtained for G/GCE, B-G/GCE, N-G/GCE and NB-G/GCE in 0.10 M pH 7.4 PBS in the absence (curve a) and presence

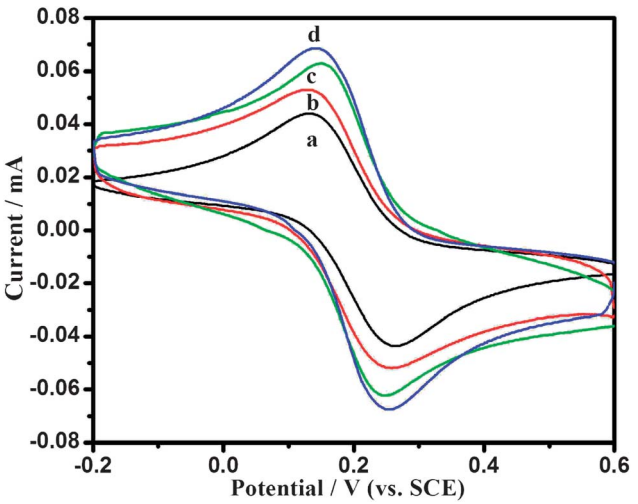

Fig. 5 CVs of G/GCE (a), B-G/GCE (b), N-G/GCE (c) and NB-G/GCE (d) in 0.1 M KCl solution containing 2.0 mM $K_3[Fe(CN)_6]/K_4[Fe(CN)_6]$.

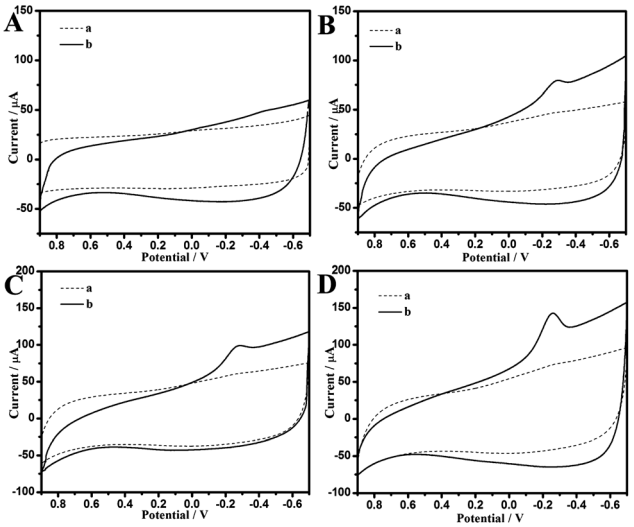

Fig. 6 CV curves of G/GCE (A), B-G/GCE (B), N-G/GCE (C) and NB-G/GCE (D) in N_2-saturated 0.1 M PBS (pH 7.4) in the absence (curve a) and presence (curve b) of 2.5 mM H_2O_2 at a scan rate of 50 mV s^{-1}.

(curve b) of H_2O_2. Of the four electrodes, BN-G/GCE was the most active, showing the lowest onset reduction potential and highest current peak at −0.247 V for H_2O_2 reduction, which was a synergistic effect resulting from the co-doping of graphene with N and B atoms. This was because not only could the isolated N and B atoms act as active sites through charge transfer with neighboring C atoms,[46] but interaction between adjacent N and B atoms also facilitated charge transfer with neighboring C atoms, as shown in Scheme 1. Consequently, NB-G possessed excellent electrochemical activity toward the redox reaction of H_2O_2. In addition, the material showed the highest peak current of all the samples prepared at different temperatures after dealing with at 900 °C (Fig. S4†), and thus it was the most promising material and was used in the subsequent experiments. These results suggested that the performance of the biosensor could be greatly improved by using suitable NB-G.

The NB-G was then used to detect the concentration of H_2O_2 at low potential with high sensitivity. The typical amperometric responses of NB-G modified electrodes for different concentrations of H_2O_2 were examined as shown in Fig. 7A. The response reached a steady signal within only 2 s and displayed a linear increase with increasing concentration from 0.5 μM to 7.5 mM, with a detection limit of 0.05 μM at a signal-to-noise ratio of 3 (Fig. 7B), which showed excellent analytical performance (Table S1†). In addition, as expected, at the same concentration of H_2O_2 (0.5 mM), the NB-G/GCE displayed an amplified response compared to the G, B-G and N-G modified GCE (Fig. S5†). These results showed that the sensors had wider linear range, relatively lower detection limit and faster current response for H_2O_2, thus it had the advantages similar to other enzymatic and non-enzymatic biosensors. Moreover, the response had also highly reproducible, as indicated by its almost unchanged current response after fifteen measurements. The relative standard deviation (RSD) of current responses for ten biofilms was less than 7.6%. The biosensor retained 90% of the initial signal following storage at 4 °C for one month, and the maximum RSD value of the reduction peak currents was 5.6%. The effects of common interfering species on the response were also examined, which showed that the H_2O_2 biosensor was free of common interferences (Table S2†). The good electrochemical properties of the enzyme-free electrode were ascribed to the architectures, large surface area, high conductivity and unhindered substance diffusion of the NB-G framework, together with the synergistic catalytic effect of co-doping which resulted in increased electron density and electron donating properties. These findings also showed that the NB-G hierarchical framework was suitable for the fabrication of H_2O_2 biosensors.

3.3. Determination of H_2O_2 released from CCRF-CEM leukemia cells

The sensor was used to determine the concentration of H_2O_2 released from CCRF-CEM leukemia cells (Fig. 8A). The release of H_2O_2 from these cells induced by fMLP was evaluated by amperometry using NB-G/GCE.[55,56] Without stimulation by fMLP, these cells did not generate any measurable signal. However, the addition of catalase, which is a H_2O_2 scavenger,[57] resulted in a sudden drop in current response followed by a progressive decrease down in signal to the background level (Fig. 8B). Control wells without CCRF-CEM cancer cells did not generate any signal following the addition of fMLP or catalase. These results verified that the response depicted in the red line was only due to H_2O_2 released from the CCRF-CEM cells. The maximum current change was around 0.061 μA, corresponding to 21 nM H_2O_2 as calculated from the calibration curve in

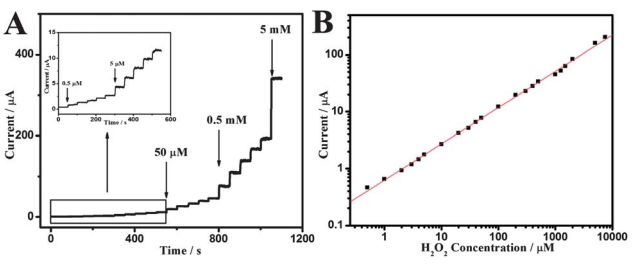

Fig. 7 (A) Current–time curve of NB-G/GCE in 0.1 M pH 7.4 PBS at an applied potential of −0.25 V. (B) The logarithmic plots of the response current *vs.* the H_2O_2 concentration.

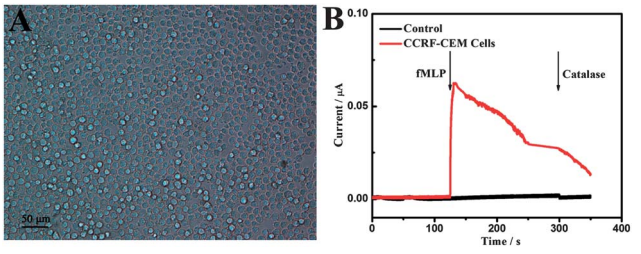

Fig. 8 (A) The bright-field microscopy image of CCRF-CEM cells (10^6 cells per mL). (B) Amperometric responses of the NB-G modified electrode in 0.1 M PBS (pH 7.4) with the addition of 1.0 μM fMLP and 300 U mL^{-1} catalase in the absence (black line) and present (red line) of CCRF-CEM cells.

Fig. 7B. Thus, upon the stimulation of 1.0 μM fMLP, the cells released more H_2O_2 at an estimated concentration of 21 fmol H_2O_2 per cell. In this regard, the proposed method could be used to study the cellular kinetics of H_2O_2. To evaluate the validity of the calculated concentration of H_2O_2 produced by CCRF-CEM cells, a recovery test was carried out. Three samples with different concentrations of CCRF-CEM cells were prepared and specific amounts of H_2O_2 were added. The average recoveries were 102.5%, 101.3% and 100.9%, and the RSDs were 2.14%, 2.87% and 3.22%, respectively (five measurements), indicating that the developed approach had high accuracy in measuring the H_2O_2 concentration released from CCRF-CEM cells.

These observations substantially confirmed that the developed NB-G with high activity represented a new sensing platform for the reliable and durable determination of H_2O_2 *in vitro* and from cancer cells, and was suitable for both intra- and extracellular H_2O_2 detection. It is expected that NB-G with good biocompatibility may provide a new electrochemical platform for the direct electrochemistry of redox-active enzymes.

4. Conclusion

We have demonstrated the preparation of a NB-G hierarchical framework through a combined microwave-activated chemical–thermal treatment, which induced an enhanced synergistic coupling effect to fabricate a highly specific biosensor for the selective measurement of H_2O_2. As an advanced electrode material, the obtained NB-G showed improved electrochemical performance compared to that of single doped graphene. The enzyme-free sensor also showed a fast response, wide linear range, low detection limit and good stability for H_2O_2 detection. The designed sensor was further used in the determination of H_2O_2 *in vitro* and released from leukemia cells and showed good application in bioelectrochemistry. This work will be beneficial for the assembly of various biomolecules into a NB-G hierarchical framework in sensing applications. It is also anticipated to open new investigations into NB-G and promote its application in addressing many issues, such as biomedical and other electronic systems.

Acknowledgements

This work was financially supported by the National Basic Research Program (2011CB933502) of China, the Doctoral Program of the Ministry of Education (20100091110023) and the National Natural Science Foundation of China (21121091).

References

1 H. Jin, D. A. Heller, M. Kalbacova, J. H. Kim, J. Zhang, A. A. Boghossian, N. Maheshri and M. S. Strano, *Nat. Nanotechnol.*, 2010, **5**, 302–309.
2 B. Halliwell and J. M. C. Gutteridge, *Free Radicals in Biology and Medicine*, Clarendon Press, Oxford, U.K., 2nd edn, 1989.
3 R. S. Arnold, J. Shi, E. Murad, A. M. Whalen, C. Q. Sun, R. Polavarapu, S. Parthasarathy, J. A. Petros and J. D. Lambeth, *Proc. Natl. Acad. Sci. U. S. A.*, 2001, **98**, 5550–5555.
4 S. DiMauro and E. A. Schon, *Annu. Rev. Neurosci.*, 2008, **31**, 91–123.
5 M. G. D. Leed, N. Wolkow, D. M. Pham, C. L. Daniel, J. L. Dunaief and K. J. Franz, *J. Inorg. Biochem.*, 2011, **105**, 1161–1172.
6 B. C. Dickinson and C. J. Chang, *J. Am. Chem. Soc.*, 2008, **130**, 9638–9639.
7 C. Lim, Y. Lee, J. Na, J. Oh, S. Her, K. Kim, K. Choi, S. Kim and I. Kwon, *Adv. Funct. Mater.*, 2010, **20**, 2644–2648.
8 Y. Song, W. Wei and X. Qu, *Adv. Mater.*, 2011, **23**, 4215–4236.
9 X. L. Sun, S. J. Guo, C. S. Chung, W. L. Zhu and S. H. Sun, *Adv. Mater.*, 2013, **25**, 132–136.
10 C. Amatore, S. Arbault, M. Guille and F. Lemaıtre, *Chem. Rev.*, 2008, **108**, 2585–2621.
11 Y. Tang, B. L. Allen, D. R. Kauffman and A. Star, *J. Am. Chem. Soc.*, 2009, **131**, 13200–13201.
12 R. D. O'Neill, J. P. Lowry, G. Rocchitta, C. P. McMahon and P. A. Serra, *TrAC, Trends Anal. Chem.*, 2008, **27**, 78–88.
13 K. S. Novoselov, A. K. Geim, S. V. Morozov, D. Jiang, Y. Zhang, S. V. Dubonos, I. V. Grigorieva and A. A. Firsov, *Science*, 2004, **306**, 666–669.
14 Y. B. Zhang, Y. W. Tan, H. L. Stormer and P. Kim, *Nature*, 2005, **438**, 201–204.
15 X. Huang, Z. Y. Yin, S. X. Wu, X. Y. Qi, Q. Y. He, Q. C. Zhang, Q. Y. Yan, F. Boey and H. Zhang, *Small*, 2011, **4**, 1876–1902.
16 C. C. Huang, C. Li and G. Q. Shi, *Energy Environ. Sci.*, 2012, **5**, 8848–8868.
17 K. P. Loh, Q. L. Bao, G. Eda and M. Chhowalla, *Nat. Chem.*, 2010, **2**, 1015–1024.
18 S. F. Huang, K. Terakura, T. Ozaki, T. Ikeda, M. Boero, M. Oshima, J. Ozaki and S. Miyata, *Phys. Rev. B: Condens. Matter Mater. Phys.*, 2009, **80**, 235410.
19 B. Biel, X. Blase, F. Triozon and S. Roche, *Phys. Rev. Lett.*, 2009, **102**, 096803.
20 H. B. Wang, T. Maiyalagan and X. Wang, *ACS Catal.*, 2012, **2**, 781–794.
21 L. S. Panchakarla, K. S. Subrahmanyam, S. K. Saha, A. Govindaraj, H. R. Krishnamurthy, U. V. Waghmare and C. N. R. Rao, *Adv. Mater.*, 2009, **21**, 4726–4730.
22 Y. Wang, Y. Y. Shao, D. W. Matson, J. H. Li and Y. H. Lin, *ACS Nano*, 2010, **4**, 1790–1798.
23 P. Wu, Z. Cai, Y. Gao, H. Zhang and C. X. Cai, *Chem. Commun.*, 2011, **47**, 11327–11329.
24 X. R. Wang, X. L. Li, L. Zhang, Y. Yoon, P. K. Weber, H. L. Wang, J. Guo and H. J. Dai, *Science*, 2009, **324**, 768–771.
25 J. Han, L. L. Zhang, S. Lee, J. Oh, K. S. Lee, J. R. Potts, J. Y. Ji, X. Zhao, R. S. Ruoff and S. J. Park, *ACS Nano*, 2013, **7**, 19–26.
26 Y. Zhao, C. G. Hu, Y. Hu, H. H. Cheng, G. Q. Shi and L. T. Qu, *Angew. Chem., Int. Ed.*, 2012, **51**, 11371–11375.
27 Z. S. Wu, W. C. Ren, L. Xu, F. Li and H. M. Cheng, *ACS Nano*, 2011, **5**, 5463–5471.
28 H. M. Jeong, J. W. Lee, W. H. Shin, Y. J. Choi, H. J. Shin, J. K. Kang and J. W. Choi, *Nano Lett.*, 2011, **11**, 2472–2477.
29 Z. Yang, Z. Yao, G. Li, G. Fang, H. Nie, Z. Liu, X. Zhou, X. A. Chen and S. Huang, *ACS Nano*, 2012, **6**, 205–211.

30 Z. S. Wu, A. Winter, L. Chen, Y. Sun, A. Turchanin, X. Feng and K. Müllen, *Adv. Mater.*, 2012, **24**, 5130–5135.
31 J. Liang, Y. Jiao, M. Jaroniec and S. Z. Qiao, *Angew. Chem., Int. Ed.*, 2012, **51**, 11496–11500.
32 S. Wang, L. Zhang, Z. Xia, A. Roy, D. W. Chang, J. B. Baek and L. Dai, *Angew. Chem., Int. Ed.*, 2012, **51**, 4209–4212.
33 Y. Zheng, Y. Jiao, L. Ge, M. Jaroniec and S. Z. Qiao, *Angew. Chem., Int. Ed.*, 2013, **52**, 3110–3116.
34 S. Nardecchia, D. Carriazo, M. L. Ferrer, M. C. Gutiérrez and F. del Monte, *Chem. Soc. Rev.*, 2013, **42**, 794–830.
35 J. M. Goran, J. L. Lyon and K. J. Stevenson, *Anal. Chem.*, 2011, **83**, 8123–8129.
36 C. Y. Deng, J. H. Chen, X. L. Chen, C. H. Xiao, L. H. Nie and S. Z. Yao, *Biosens. Bioelectron.*, 2008, **23**, 1272–1277.
37 D. Li, M. B. Müller, S. Gilje, R. B. Kaner and G. G. Wallace, *Nat. Nanotechnol.*, 2011, **3**, 101–105.
38 T. W. Lin, C. Y. Su, X. Q. Zhang, W. J. Zhang, Y. H. Lee, C. W. Chu, H. Y. Lin, M. T. Chang, F. R. Chen and L. J. Li, *Small*, 2012, **8**, 1384–1391.
39 L. J. Ci, L. Song, C. H. Jin, D. Jariwala, D. X. Wu, Y. J. Li, A. Srivastava, Z. F. Wang, K. Storr, L. Balicas, F. Liu and P. M. Ajayan, *Nat. Mater.*, 2010, **9**, 430–435.
40 H. F. Qian, X. Q. L. Li and J. C. Ren, *J. Phys. Chem. B*, 2006, **110**, 9034–9040.
41 Y. Zhu, S. Murali, M. D. Stoller, K. J. Ganesh, W. Cai, P. J. Ferreira, A. Pirkle, R. M. Wallace, K. A. Cychosz, M. Thommes, D. Su, E. A. Starch and R. S. Ruoff, *Science*, 2011, **332**, 1537–1541.
42 Z. Jin, J. Yao, C. Kittrell and J. M. Tour, *ACS Nano*, 2011, **5**, 4112–4117.
43 X. Yang, L. Liu, M. Wu, W. Wang, X. Bai and E. Wang, *J. Am. Chem. Soc.*, 2011, **133**, 13216–13219.
44 E. A. Ekimov, V. A. Sidorov, E. D. Bauer, N. N. Mel'nik, N. J. Curro, J. D. Thompson and S. M. Stishov, *Nature*, 2004, **428**, 542–545.
45 C. H. Choi, S. H. Park and S. I. Woo, *ACS Nano*, 2012, **6**, 7084–7091.
46 L. J. Yang, S. J. Jiang, Y. Zhao, L. Zhu, S. Chen, X. Z. Wang, Q. Wu, J. Ma, Y. W. Ma and Z. Hu, *Angew. Chem., Int. Ed.*, 2011, **50**, 7132–7135.
47 N. Mohanty, A. Nagaraja, J. Armesto and V. Berry, *Small*, 2010, **6**, 226–231.
48 J. L. Zhang, H. J. Yang, G. X. Shen, P. Cheng, J. Y. Zhang and S. W. Guo, *Chem. Commun.*, 2010, **46**, 1112–1114.
49 K. N. Kudin, B. Ozbas, H. C. Schniepp, R. K. Prud'homme, I. A. Aksay and R. Car, *Nano Lett.*, 2008, **8**, 36–41.
50 Z. Z. Lv, X. Yang and E. K. Wang, *Nanoscale*, 2013, **5**, 663–670.
51 B. P. Vinayan, R. Nagar, N. Rajalakshmi and S. Ramaprabhu, *Adv. Funct. Mater.*, 2012, **22**, 3519–3526.
52 M. Pumera, *Chem. Soc. Rev.*, 2010, **39**, 4146–4157.
53 Q. Zeng, J. S. Cheng, L. H. Tang, X. F. Liu, Y. Z. Liu, J. H. Li and J. H. Jiang, *Adv. Funct. Mater.*, 2010, **20**, 3366–3372.
54 X. H. Cao, Z. Y. Zeng, W. H. Shi, P. R. Yep, Q. Y. Yan and H. Zhang, *Small*, 2013, **9**, 1703–1707.
55 C. X. Guo, X. T. Zheng, Z. S. Lu, X. W. Lou and C. M. Li, *Adv. Mater.*, 2010, **22**, 5164–5167.
56 X. L. Sun, S. J. Guo, Y. Liu and S. H. Sun, *Nano Lett.*, 2012, **12**, 4859–4863.
57 F. Xiao, Y. Q. Li, X. L. Zan, K. Liao, R. Xu and H. W. Duan, *Adv. Funct. Mater.*, 2012, **22**, 2487–2494.

